Orthogonal chemical functionalization of patterned Au/TiW substrate for selective immobilization of nanoparticles

Jian Zhang, Didier Léonard, Radoslaw Mazurczyk, Christelle Yeromonahos, Virginie Monnier, Thomas Gehin, Stéphane Monfray, Yann Chevolot, Jean-Pierre Cloarec

Orthogonal chemical functionalization of patterned Au/TiW substrate for selective immobilization of nanoparticles

Jian Zhang[1], Didier Léonard[2], Radoslaw Mazurczyk[1], Christelle Yeromonahos[1], Virginie Monnier[1], Thomas Géhin[1], Stéphane Monfray[3], Yann Chevolot[1] and Jean-Pierre Cloarec[1]

[1] Université de Lyon, Institut des Nanotechnologies de Lyon (INL) − UMR CNRS 5270, Ecole Centrale de Lyon, 36 Avenue Guy de Collongue, 69134 Ecully cedex, France.

[2] Univ Lyon, CNRS, Université Claude Bernard Lyon 1, ENS de Lyon, Institut des Sciences Analytiques, UMR 5280, 5, rue de la Doua, F-69100 Villeurbanne, France.

[3] STMicroelectronics SA, 850, rue Jean Monnet, 38926, Crolles, France.

Email: yann.chevolot@ec-lyon.fr; jean-pierre.cloarec@ec-lyon.fr

Abstract

A current evolution of nanobiosensors stresses the interest of multi-material nanopatterned surfaces, for enhancing sensing performances. Besides, titanium tungsten (TiW) is mastered routinely implemented in nanoelectronic devices, in a reproducible way and at industrial production scales. Such material may be envisioned for being used in (bio)chemical nanoelectronic sensors, but the surface functionalization of such material has still to be studied. In the present article, orthogonal chemical functionalization of patterned Au on titanium tungsten (TiW) substrates have been explored for the first time to our knowledge. Surface functionalizations were assessed by X-ray photoelectron spectroscopy (XPS), polarization modulation infrared reflection-absorption spectroscopy (PMIRRAS) and time-of-flight secondary ion mass spectrometry (ToF-SIMS) imaging. Au/TiW patterned substrates were functionalized with mercapto-undecamine. Thanks to the orthogonality of thiol/Au versus phosphonic acid/TiW reactions, only Au features were modified leading to the amine derivatized surface. It allowed localizing carboxy-functionalized nanoparticles by electrostatic interaction on Au with a selectivity above 10 compared to TiW.

Keywords

titanium tungsten, TiW, nanoelectronics, orthogonal chemical functionalization, surface functionalization, nanoparticles

Introduction

In its most classical description, a (bio)chemical sensor can be described as the association of a receptor and a transducer. The receptor is a layer composed or molecular probes (e.g. antibody, oligonucleotide, or chemical moieties) chosen for their affinity towards a precise (bio)chemical target to be detected. The transducer is a device aimed at translating probe/target interactions into a measurable signal. For years, transducers turn from a one-dimensional structuration to two dimensional or three dimensional patterns with nanometric "hot spots" to enhance sensing performance. For example, nanobiosensors based on nanowires Field Effect Transistors (FETs) transducers are expected to exhibit a higher sensitivity than FET biosensors [l]. However, the size reduction of the transducer (e.g. nanometric size FET structure) can be useful only if molecular targets are captured specifically on the sensing area, and not trapped elsewhere on non-sensitive zones (e.g. fluidic circuits, nanosensor packaging material). If molecular probes are unintentionally immobilized outside of transducing area, they may capture molecular targets and prevent them to reach the transducer: these targets cannot contribute to the useful signal. It is therefore important to ensure that (1) molecular probes bind correctly on transducing zone; (2) molecular probes and molecular targets should not bind to any other part of the sensing device [2].

FET (bio)chemical sensors are still a subject of academic and industrial research; indeed, reduction of the sensor's transducer area and/or use of embedded electronic amplification devices are currently studied [3, 4]. As stated above, for such nanodevices, higher sensitivity will also be fully effective only if molecular targets can be captured onto nanosize transducer area, and repelled elsewhere in the sensing full device [5]. It is therefore important to explore strategies for fabricating nanoelectronic sensors with different surface materials, with at least one material providing the transducer zone, and at least another material providing a packaging environment. Gold and silica have already been explored as model materials for fabricating surfaces with two different surface functionalization reactions, using orthogonal surface reactions [6-8].

Orthogonal grafting of different molecules onto patterned substrates was first proposed in 1989, for macroscopic scale patterns. It offered a versatile method for controlling the interfacial properties of each material [9, 10]. Nowadays orthogonal chemical functionalizations at the submicronic scale are still based on organic molecules bearing different anchoring groups that will react selectively with different materials on nanopatterned substrates. This strategy combines the top-down fabrication process such as lithography which allows the creation of well-defined micro or nanostructures and bottom-up process such as molecules organolayers formation which allows the modifying the functionalities. If molecules used for orthogonal chemical functionalization are truly selective for each material, it offers the perspective of controlling and modifying the characteristics of each material surfaces and incorporating new functionalities on the defined nanofabricated devices [11-15]. The ability to chemically modify specific zones of a substrate can provide several advantages. In the field of chemical nanosensors, orthogonal chemical functionalization has been studied. Different combinations of chemical compounds and inorganic substrates have been used in such functionalization protocols, such as metal oxide/SiO_2 [11, 16], Au/metal oxide [17, 18], or Au/SiO_2 [19-22] templates selectively functionalized with thiols, phosphonic acids, carboxylic acids or silanes.

Besides, titanium tungsten (TiW) is well mastered materials commonly used in nanoelectronic industry [23-29]. It is implemented in nanoelectronic devices on an industrial scale, with a very high control on its characteristics. Among different materials potentially used for elaborating (bio)chemical sensors, TiW could therefore be envisioned as one of the materials to be explored for nanoelectronic transducers.

In the present article, we explored how orthogonal chemical functionalization of a substrate including TiW and another material could be implemented. As a first practical assessment, we studied TiW/Au heterogeneous surfaces. TiW Thiol based chemistry and phosphonic acid based chemistry were used for the selective derivatization of Au and TiW, respectively. Orthogonal chemical functionalization was verified by direct characterization tools using X-ray photoelectron spectroscopy (XPS), polarization modulation infrared reflection absorption spectroscopy (PM-IRRAS) and time-of-flight secondary ion mass spectrometry (ToF-SIMS) imaging. In addition, we assessed with SEM imaging how Au/TiW selectively functionalized surfaces enable to specifically immobilize nanoparticles on Au patterns.

Experimental Section

Materials: 1H, 1H, 2H, 2H-Perfluorodecanethiol (F-thiol) 97% was purchased from Sigma-Aldrich. 1H,1H,2H,2H-Tridecafluorooct-1-yl)phosphonic acid (F-Phosphonate) was purchased from SiKÉMIA. Dichloromethane (DCM) 99.9% was purchased from Sigma-Aldrich then degassed and dried over molecular sieves. Isopropanol 99.9% was purchased from Fluka. 11-mercapto-1-undecylamine (MUAM) 99% and ethanol 99.8% were purchased from Sigma-Aldrich. Carboxylatex particles (300 nm diameter, 3% solids, product code: 02131) were purchased from Ademtech.

Substrate patterning: Macroscale patterned Au/TiW substrates S_1 and S_2 were prepared using the following protocol: the surfaces consisted of a 2 cm^2 TiW substrate onto which half of the surface was covered by gold thin film (5 nm chromium and 200 nm gold). Microscale patterned Au/TiW substrates S_3, S_4 and S_5 were prepared using UV lithography process to define squares with typical dimensions ranging from 100 μm to 600 μm. Chromium (5 nm) and gold (50 nm) were deposited by electron beam evaporation (Leybold, 1.5×10^{-6} Torr, 6 kV, 2 Å/s). After lift-off, the samples were cleaned by oxygen plasma treatment (HARRICK) at the oxygen flow rate of 14 ml/min, RF power level of 38 W for 5 minutes to ensure that no residual resist remained on the surface.

Surface functionalization:

Patterned substrates S_1 and S_3 were functionalized by F-thiol using the following protocol: substrates were immersed in 25 ml dried DCM containing 100 µl F-thiol (14 mM) for 48 hours. Then the samples were rinsed with DCM for 5 min under ultrasound (Branson, 42 kHz, 100 W) followed by a stream of ultrapure water and dried with nitrogen flow. Patterned substrates S_2 and S_4 were functionalized by F-phosphonic acid using the following protocol: substrates were immersed in 20 ml ultrapure water containing 8.5 mg F-phosphonic acid (1 mM) for 16 hours. The substrates were then rinsed with isopropanol for 5 min under ultrasound (Branson, 42 kHz, 100 W) followed by a stream of ultrapure water and dried with nitrogen flow. Patterned substrates S_5 was functionalized by MUAM using the following protocol: substrates were immersed in a previously degassed 1 mM ethanolic solution of MUAM for 4 hours and then rinsed 5 min in ethanol under sonication (Branson, 42 kHz, 100 W) to remove potentially adsorbed multilayers, followed by 5 min rinse in ultrapure water and then dried under nitrogen flow.

Nanoparticles trapping: 20 µl of carboxylate-functionalized nanoparticles dispersion were suspended in 2 ml of PBS-1X adjusted to pH 7.4 in a centrifuge tube. S_5 substrates functionalized by MUAM were maintained vertically in the centrifuge tube fully immersed in the nanoparticles dispersion without stirring at room temperature. No sedimentation of colloidal dispersions was observed overnight. The immobilized S_5 substrates were rinsed twice with ultrapure water and dried under nitrogen. A control sample without functionalization was immersed in a dispersion of carboxylate-functionalized nanoparticles overnight and rinsed in the same way.

Characterizations: Polarization-modulation infrared reflection absorption spectroscopy (PM-IRRAS) spectra was recorded on macroscopic substrates S_1 and S_2 using a Nicolet 6700 FTIR spectrometer from Thermo Scientific coupled to a Hinds Instrument PEM-100 ZnSe photoelastic modulator driven at 50 kHz (polarization switch from p to s at 100 kHz). The dimensions of TiW and Au macropatterns were largely higher than IR beam, so that each material of a same substrate could be characterized individually. X-ray Photoelectron Spectroscopy (XPS) measurements on macropatterned substrates S_1 and S_2 were performed using a focused monochromatized X-ray source (Al Kα = 1486.6 eV). Spectra acquisitions were performed under ultrahigh vacuum conditions (UHV, 10^{-9} Torr). Take-off angle was 90° relative to the substrate surface. The pass energies were 100 eV and 20 eV for wide-scan and high-resolution elemental scans, respectively. The data reduction was performed with CasaXPS software. The dimensions of TiW and Au patterns were largely higher than XPS beam, so that each material of a same substrate could be characterized individually. Time-of-flight secondary ion mass spectrometry (ToF-SIMS) measurements were performed on micropatterned substrates S_3 and S_4 with a Physical Electronics TRIFT III instrument (Physical Electronics, Chanhassen, MN) operated with a pulsed Au ion gun (ion current of 2 nA) over a 300 µm × 300 µm area. The ion dose was kept below the static conditions limits. Data were analyzed using WinCadence software. Mass calibration was performed on hydrocarbon secondary ions. Scanning Electron Microscopy (SEM) images were performed on micropatterned substrates S_5 before and after nanoparticles trapping with a Mira3 SEM from TESCAN. It was operated with an acceleration voltage of 5 kV, a current beam of 250 µA with a detection of secondary electrons. SEM image analysis with ImageJ software allowed us to compute quantitative data. At least three measurements were performed on different locations, thus providing triplicate quantitative images.

Results and discussion

The ability to address large sets of molecules or nano-objects onto precise spots of a surface may enable to fabricate new nanosystems that could not be created using classical top-down fabrication methods. Such way of fabrication is envisioned for elaborating exotic new nanodevices, by associating (1) the versatility provided by materials science for creating new nano-objects (e.g. quantum dots, nanowires, nanotubes…) and (2) the possibility to organize these nano-objects onto sites predefined using classical approaches (e.g. nanolithography and lift-off, nanoimprint…). Different approaches have been explored by various groups for placing nano-objects onto micro and nanosystems, using for instance capillary forces, microcontact printing or electric fields [2, 5-7, 30].

Among the various approaches explored for locating and anchoring nano-objects or molecules onto micronic or nanometric zones, orthogonal surface functionalizations provide a powerful tool to bridge the gap between top-down and bottom-up nanofabrication methods [5, 19]. By adjusting their surface chemistry, we can enable whole sets of different molecules and/or nano-objects to be selectively deposited and organized onto well-defined (sub)micronic anchoring sites on macroscopic systems. This potentially enables the development of unprecedented systems in different fields such as photonics, electronics, chemical sensors and biosensors.

In the present article, we study functionalization of TiW. TiW is a material well controlled by nanoelectronic industry, and it is commonly used in nanoelectronics structures as diffusion barrier. Indeed, since TiW can be implemented in a very reproducible way for mass production of nanoelectronic structures, it could be used not only for its barrier properties, but as a surface material to be used close to nanotransducers in new generations of ion sensitive field-effect transistor (ISFETS) [3, 4]. At the stage of these studies, we explored surface functionalization of Au/TiW mixed surfaces as a first validation with micronic size features.

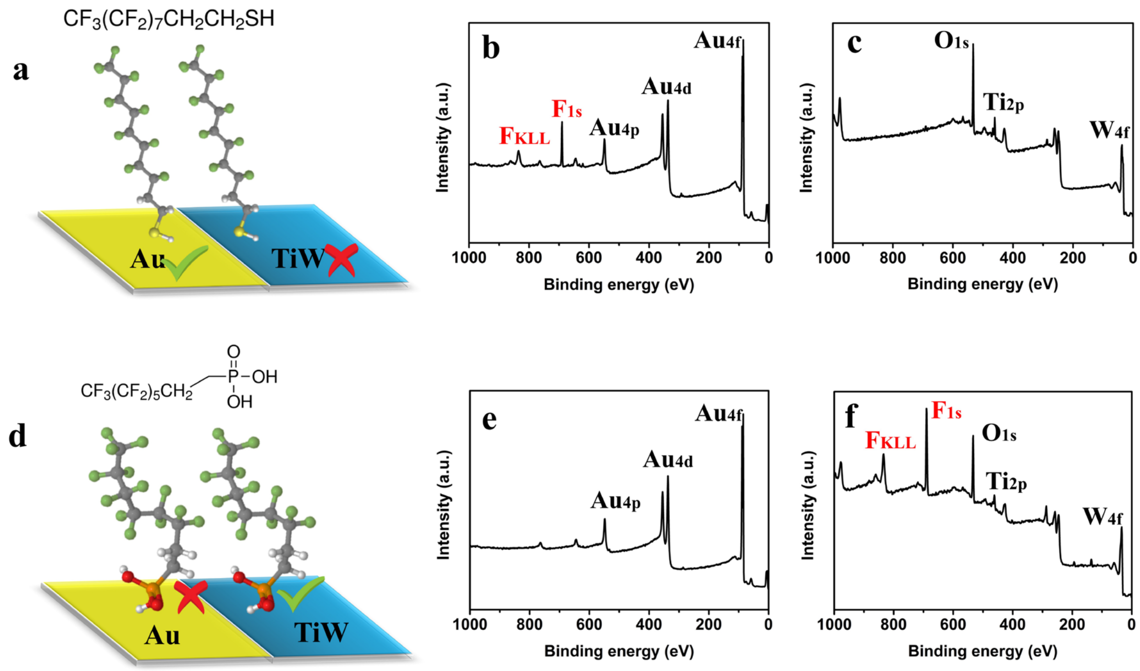

Figure 1 *(a) Scheme of macropatterned Au on TiW substrates functionalized with F-thiol. The corresponding XPS survey spectra measured on Au and TiW are displayed in (b) and (c), respectively. (d) Scheme of macropatterned Au on TiW substrates functionalized with F-phosphonic acid. The corresponding XPS survey spectra measured on Au and TiW are displayed in (e) and (f), respectively.*

Functionalized organolayers were firstly implemented on macroscale patterned substrates, and characterized by XPS and PM-IRRAS measurements. Such surfaces consisted of a TiW substrate onto which half of the surface was covered by Au thin film to form macroscale patterns. The patterned Au/TiW substrates were functionalized by either 1H,1H,2H,2H-perfluorodecanethiol (F-thiol, figure 1a) or (1H,1H,2H,2H-tridecafluorooct-1-yl)phosphonic acid (F-phosphonic acid, figure 1d) and were analyzed using XPS. Survey and high-resolution spectra were recorded for areas corresponding to either Au or TiW. Figure 1b and Figure 1c show the XPS survey spectra of Au and TiW areas of macropatterned substrates after incubation with perfluorinated thiol. On Au, fluorine was clearly evidenced by the F1s and FKLL peaks, showing the presence of the perfluorinated thiol. On the contrary, fluorine could not be observed on TiW. After incubation of macropatterned substrate with F-phosphonic acid, F1s and FKLL peaks were only observed on TiW. Such peaks were not observed on Au (figure 1e, f). High resolution XPS spectrum of F1s and C1s are given in supporting information. They confirmed the component of F-thiol functionalized Au (figure Sup1a, b). Indeed, after incubation with perfluorinated thiol, contribution at 293.0 eV, 291.5 eV and 290.0 eV can be attributed to CF_3, CF_2-CF_2 and CH_2-CF_2, respectively. On TiW, the only contribution (284.8 eV) observed on the C1s corresponded to hydrocarbon (figure Sup1c). High resolution XPS spectrum of F1s and C1s confirmed the component of F-phosphonic acid functionalized TiW (figure Sup1 d, e). After incubation with the perfluorinated phosphonic acid, the contributions at 293.0 eV, 291.5 eV and 290.0 eV attributed to CF_3, CF_2-CF_2 and CH_2-CF_2 were only observed on TiW. On Au, the only contribution (284.8 eV) observed on the C1s corresponded to hydrocarbon (figure Sup1f).

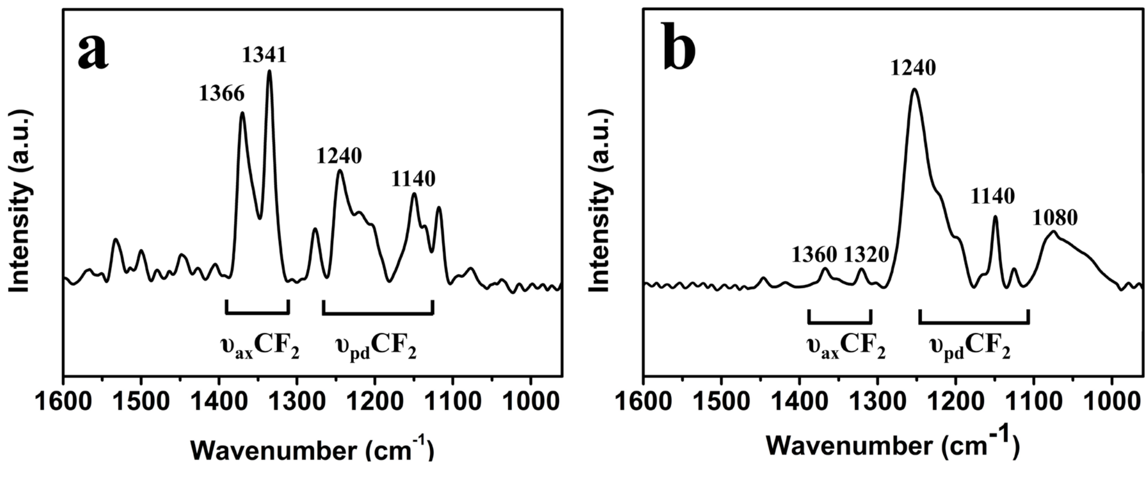

Figure 2 (a) PM-IRRAS spectra recorded on Au of macropatterned substrates functionalized with F-thiol. (b) PM-IRRAS spectra recorded on TiW of macropatterned substrates functionalized with F- phosphonic acid.

PM-IRRAS spectra were also conducted on similar orthogonally functionalized surfaces, figure 2a displays the PM-IRRAS spectra corresponding to Au area of macroscale patterned substrate functionalized with F-thiol. It has been found that the CF stretching vibrations region from 1000 cm^{-1} to 1600 cm^{-1} were present on Au area. Additionally, on TiW, no CF stretching vibrations peaks were observed indicating that the F-thiol was below PM-IRRAS detection limit on TiW (data not displayed). PM-IRRAS spectra of TiW area following incubation with F-phosphonic acid is displayed in figure 2b. A broad peak at from 1000 cm^{-1} to 1100 cm^{-1} was attributed to the P-O bend [31, 32]. It has been found that CF stretching vibrations region from 1000 cm^{-1} to 1600 cm^{-1} were present on TiW area. Additionally, on Au, no CF stretching vibrations peaks were observed (data not displayed). In detail, the bands around 1240 cm^{-1} and 1140 cm^{-1} were assigned to asymmetric and symmetric CF_2 stretching vibrations, which are referred to perpendicular CF_2 stretching bands $\upsilon_{pd}CF_2$. Peaks at 1320 cm^{-1} and 1366 cm^{-1} are referenced as the axial CF_2 stretching vibration bands $\upsilon_{ax}CF_2$ [33, 34].

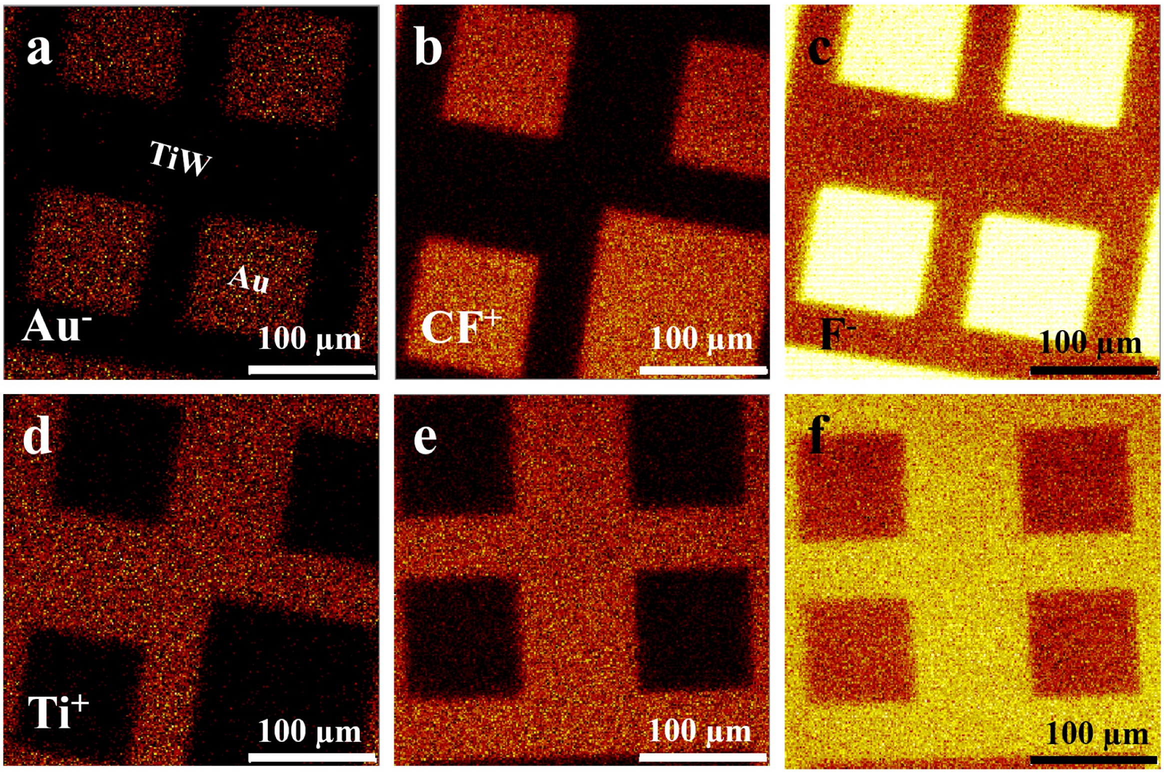

Figure 3 *ToF-SIMS images (300 × 300 µm^2; scale bar, 100 µm) of Au$^-$, Ti$^+$, CF$^+$ and F$^-$ ions of micropatterned Au/TiW substrates functionalized with F-thiol (a-c) or F-phosphonic acid (d-f).*

In order to test the orthogonality of functionalization on the micropatterned substrates, fluorine mapping was conducted using ToF-SIMS, which has been shown to be especially well-suited for the characterization of chemically patterned surfaces [35-37]. As shown in figure 3, CF$^+$ and F$^-$ were imaged on micropatterned substrates functionalized after incubation with F-thiol or F-phosphonic acid. In the case of F-thiol functionalization, the F$^-$, CF+ and Au$^-$ ions originated from the same areas, whereas on the surrounding TiW the fluorine associated ions had weak intensities (figure 3a-c). Opposite observations can be drawn when the substrate was incubated with F-phosphonic acids: F^- and CF^+ signals are issued from the TiW areas (figure 3d-f). In each case, only fluorine is present on the Au squares or the surrounding TiW but not on both, which demonstrates the good orthogonality of the functionalization.

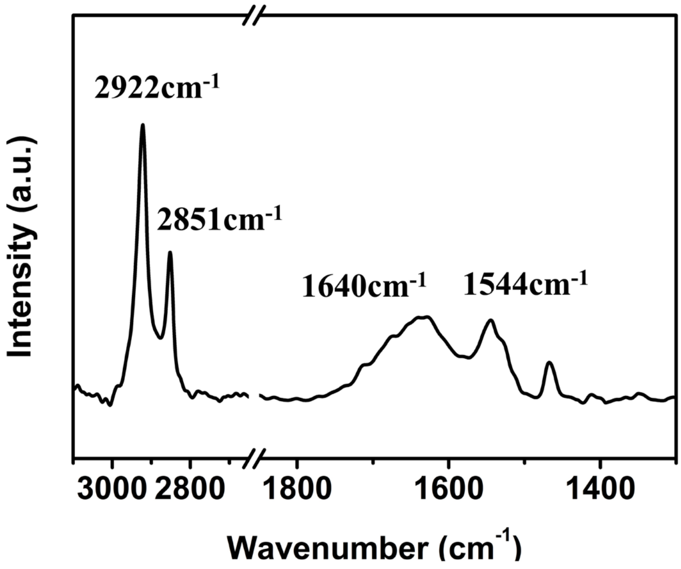

Figure 4 *PM-IRRAS spectra of Au functionalized by MUAM.*

It has been shown that thiol molecules could be selectively addressed on Au areas rather than TiW ones. In the following, we demonstrate that thiol organolayer on Au can be used for the selective capture of nanoparticles on Au/TiW patterned substrates. Amino terminated thiol (MUAM) functionalized Au substrates were characterized by PM-IRRAS in figure 4. The spectra showed the bands at 2922 cm^{-1} and 2851 cm^{-1} assigned to the asymmetric and symmetric vibration of CH_2. Furthermore, the position of the symmetric and asymmetric CH_2 stretching bands indicated the close-packing of the alkyl chains in the monolayers. It also showed N-H deformation vibration modes at 1640 cm^{-1} and 1544 cm^{-1}. These bands are associated with the protonated form of the primary amine group NH_3^+ [38]. High-resolution S2p spectrum can be attributed to two S2p doublet: $S_{3/2}$ and $S_{1/2}$ contributions with the main signals $S2p_{3/2}$ centered at 162.2 eV and 163.9 eV (figure Sup2a). The first doublet can be assigned to sulfur bound to Au surface atom, and the second indicates unbound sulfur, present despite the intensive rinsing of samples [39, 40]. Due to the dissymmetry of the N1s, two contributions seem to be present on the high-resolution N1s spectra, which were associated with a free amine $-NH_2$ group at 399.8 eV and protonated amine $-NH_3^+$ group at 401.7 eV, respectively (figure Sup2b) [41]. The results in combination with the selectivity of thiol for Au versus TiW allowed the selective trapping of nanoparticles onto Au features by electrostatic interactions.

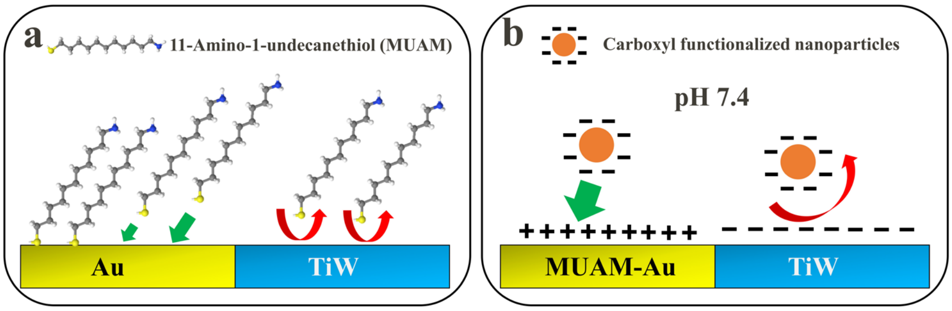

Figure 5 *(a) Schematic representation of micropatterned Au/TiW substrates selectively functionalized by MUAM. (b) Schematic representation of carboxyl functionalized nanoparticles immobilized on the micropatterned Au/TiW substrates selectively functionalized by MUAM (not to scale).*

The carboxylated nanoparticles were incubated with MUAM modified micropatterned Au/TiW substrates. The experiment was conducted under pH 7.4. At this pH, the amines were expected to be protonated while carboxyl groups of the nanoparticles were expected to be deprotonated. MUAM functionalized Au areas were used to address the carboxylated nanoparticles by attractive electrostatic interactions between positively charged amines (NH_3^+) and negatively charged carboxylic acids (COO^-) at pH = 7.4 (respective pKa of amines and carboxylic acids are around 9-10 and 3-4). The scheme of selective functionalization of MUAM on Au patterns versus TiW and specific immobilization of nanoparticles on Au features is shown in figure 5.

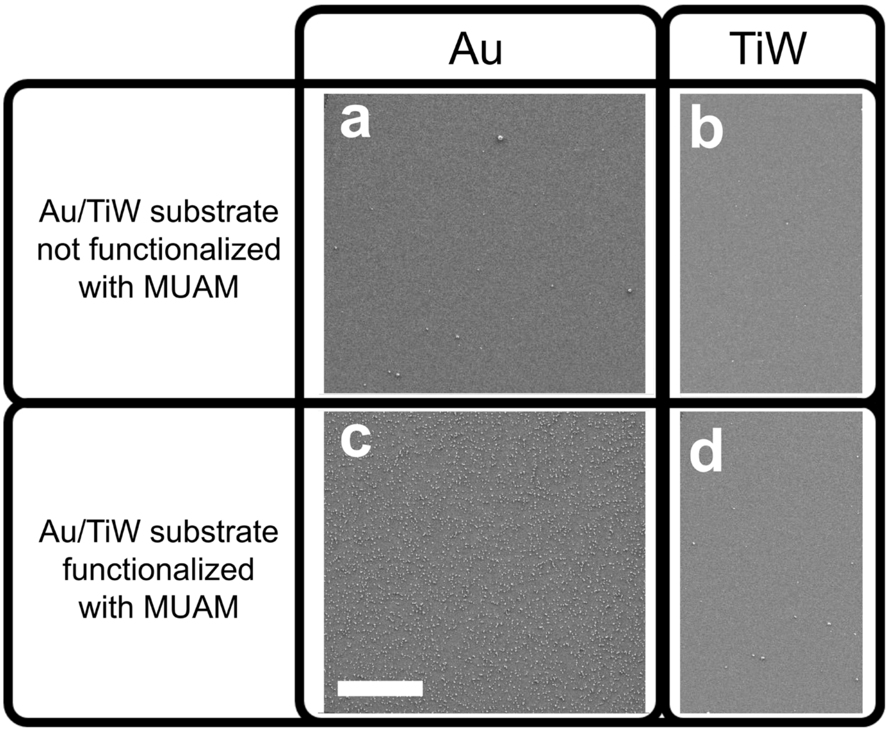

***Figure** 6. Influence of MUAM functionalization on the capture of carboxylated nanoparticles on mixed Au/TiW substrate. Top: SEM images of Au/TiW substrate not functionalized with MUAM. (a): Au zone; (b): TiW zone. Bottom: SEM images of Au/TiW substrate functionalized with MUAM. (c): Au zone; (d): TiW zone. Nanoparticles were only significantly captured for Au functionalized with MUAM (image c). Scale bar =20 µm.*

After nanoparticles deposition, SEM images were taken to determine the nanoparticles positions as shown in figure 6. It can be seen that compared to the control sample without MUAM functionalization (figure 6a, b), carboxylate nanoparticles were selectively placed on Au patterns (figure 6c) rather than on TiW (figure 6d) after the selective functionalization of MUAM organolayer. The result is consistent with the selectivity of thiol for Au versus TiW, allowing the selective trapping of nanoparticles onto MUAM functionalized Au features only. More images of MUAM functionalized Au/TiW patterned substrates after nanoparticles deposition with different areas are provided in the supporting information (figure Sup3, Sup4 and Sup5). SEM images were analyzed with ImageJ software to compute the specific trapping of nanoparticles on the Au regions and non-specific adsorption on surrounding TiW. Au and TiW regions were using binarization with appropriate threshold values, enabling to distinguish nanoparticles from background. On both regions, the percentage of nanoparticles pixels were computed and correspond to the specific trapping and non-specific adsorption of nanoparticles.

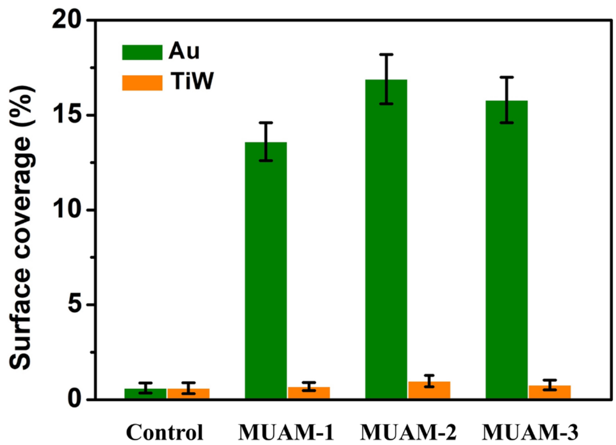

***Figure** 7 Surface coverage of nanoparticles on Au and TiW regions of the Au/TiW patterned surfaces for three different samples MUAM-1, 2 and 3 functionalized with MUAM. SEM was used to characterize three different zones of each material of each sample. Errors bars indicate standard deviation for the different zones of a same material, on a same sample.*

The results of selectively trapped nanoparticles on patterned substrates were summarized in figure 7. Three different samples (MUAM 1, 2, 3) were prepared for each nanoparticles solution with the same procedure. SEM images showed that non-specific adsorption on control sample corresponding to a non-functionalized surface is around 10-fold lower than Au modified with MUAM. Indeed, since nanoparticles deposition was performed at pH=7.4, the TiW surface as well as the carboxyl functionalized nanoparticles were expected to be negatively charged (point of zero charge of TiW is around 3). Electrostatic repulsion probably accounts for the low non-specific adsorption of the colloids onto the TiW surface. Most importantly, the number of nanoparticles on Au was found to be one order of magnitude higher than the one observed on TiW. Error bars in figure 7 correspond to surface coverage standard deviation. Each standard deviation was calculated using three different regions of a same material from a same sample. Calculated surface coverage standard deviations were approximately +/- 1.5 % for gold squares. Some surface coverage was found heterogeneous for a few zones. This was attributed to defects in substrate fabrication (e.g. tweezer traces, resist traces) and or aggregations of particles on some sites of the surface. Nonetheless, this +/- 1.5 % of standard deviation for surface coverage was found to be rather constant for a majority of imaged surfaces. Supporting information provides more SEM (figure Sup3) and optical microscopy images (figure Sup4) showing the repartition of nanoparticles on gold squares ranging from 100 µm to 600 µm long. Electrostatic attraction between the negatively charged nanoparticles and the positively charged MUAM-modified Au was accounted for the trapping of the nanoparticles, which showed the efficiency of surface chemical functionalization to selectively anchor nanoparticles onto predefined Au regions of a heterogeneous TiW substrate.

Conclusions

In this paper, we reported the selective and independent chemical functionalization of TiW and Au areas on Au/TiW patterned substrates thanks to the orthogonality of phosphonic acid and thiol molecules reactivity. Direct characterizations using XPS, PM-IRRAS and ToF-SIMS imaging provided evidence of the chemical orthogonality. Nanoparticles were precisely anchored on Au patterns through selective chemical functionalization of Au regions allowing for electrostatic trapping. The specific capturing of nanoparticles on gold was increased by one order of magnitude in respect to non-specific adsorption on TiW. This method is being developed to eventually anchor of nano-objects or biomolecules onto large arrays of nanoscale nanoelectronic transducers. We expect to broaden the library of nanosensors based on TiW transducers with multi-materials patterned surfaces (e.g. Si_3N_4 or SiO_2).

References

[1] F. Patolsky, G.F. Zheng, O. Hayden, M. Lakadamyali, X.W. Zhuang, C.M. Lieber. Electrical detection of single viruses. *PNAS*, **2004**, *101,* 14017–14022.

[2] F. Palazon, V. Monnier, Y. Chevolot, É. Souteyrand, J.P. Cloarec. NANOTRAPS: different approaches for the precise placement of micro and nano-objects from a colloidal dispersion onto nanometric scale sites of a patterned macroscopic surface. *Journal of Colloid Science and Biotechnology*, **2013**, *2*, 249–262.

[3] L. Rahhal, G.T. Ayele, S. Monfray, J.P. Cloarec, B. Fornacciari, E. Pardoux, C. Chevalier, S. Ecoffey, D. Drouin, P. Morin, P. Garnier, F. Boeuf, A. Souifi. High sensitivity pH sensing on the BEOL of industrial FDSOI transistors. *Solid-State Electronics*, **2017**, *134*, 22–29.

[4] G.T. Ayele, S. Monfray, S. Ecoffey, F. Boeuf, J.P. Cloarec, D. Drouin, A. Souifi. Ultrahigh-sensitive CMOS pH sensor developed in the BEOL of standard 28 nm UTBB FDSOI. *IEEE Journal of the Electron Devices Society*, **2018**, *6*, 1026–1032.

[5] F. Palazon, P. Rojo-Romeo, A. Belarouci, C. Chevalier, H. Chamas, É. Souteyrand, J.P. Cloarec. Site-selective self-assembly of nano-objects on a planar substrate based on surface chemical functionalization. *Nanopackaging: From Nanomaterials to the Atomic Scale, Springer, Cham*, **2015**, 93–112.

[6] C.H. Lalander, Y.H. Zheng, S. Dhuey, S. Cabrini. DNA-directed self-assembly of gold nanoparticles onto nanopatterned surfaces: controlled placement of individual nanoparticles into regular arrays. *ACS Nano*, **2010**, *4*, 6153–6161.

[7] E. Penzo, M. Palma, R.S. Wang, H.G. Cai, M. Zheng, S.J. Wind. Directed assembly of end-functionalized single wall carbon nanotube segments. *Nano letters*, **2015**, *15*, 6547–6552.

[8] F. Palazon, P. Rojo-Romeo, C. Chevalier, T. Géhin, A. Belarouci, A. Cornillon, F. Zuttion, M. Phaner-Goutorbe, É. Souteyrand, Y. Chevolot, J.P. Cloarec. Nanoparticles selectively immobilized onto large arrays of gold micro and nanostructures through surface chemical functionalizations. *J. Colloid Interface Sci.*, **2015**, *447*, 152–158.

[9] P.E. Laibinis, J.J. Hickman, M.S. Wrighton, G.M. Whitesides. Orthogonal self-assembled monolayers: alkanethiols on gold and alkane carboxylic acids on alumina. *Science*, **1989**, *245*, 845–847.

[10] T.J. Gardner, C.D. Frisbie, M.S. Wrighton. Systems for orthogonal self-assembly of electroactive monolayers on Au and ITO: an approach to molecular electronics. *J. Am. Chem. Soc.*, **1995**, *117*, 6927–6933.

[11] R. Michel, I. Reviakine, D. Sutherland, C. Fokas, G. Csucs, G. Danuser, N.D. Spencer, M. Textor. A novel approach to produce biologically relevant chemical patterns at the nanometer scale: selective molecular assembly patterning combined with colloidal lithography. *Langmuir*, **2002**, *18*, 8580–8586.

[12] M. Bergkvist, N. Niamsiri, A.D. Strickland, C.A. Batt. Substrate selective patterning on lithography defined gold on silica: effect of end-group functionality on intermolecular layer formation. *Surf. Sci.*, **2008**, *602*, 2121–2127.

[13] T.A. Gschneidtner, S. Chen, J.B. Christensen, M. Käll, K. Moth-Poulsen. Toward plasmonic biosensors functionalized by a photoinduced surface reaction. *J. Phys. Chem. C*, **2013**, *117*, 14751–14758.

[14] N. Zhang, Y.J. Liu, J. Yang, X.D. Su, J. Deng, C.C. Chum, M.H. Hong, J.H. Teng. High sensitivity molecule detection by plasmonic nanoantennas with selective binding at electromagnetic hotspots. *Nanoscale*, **2014**, *6*, 1416–1422.

[15] L. Feuz, M.P. Jonsson, F. Höök. Material-selective surface chemistry for nanoplasmonic sensors: optimizing sensitivity and controlling binding to local hot spots. *Nano Lett.*, **2012**, *12*, 873–879.

[16] R. Michel, J.W. Lussi, G. Csucs, I. Reviakine, G. Danuser, B. Ketterer, J.A. Hubbell, M. Textor, N.D. Spencer. Selective molecular assembly patterning: a new approach to micro- and nanochemical patterning of surfaces for biological applications. *Langmuir*, **2002**, *18*, 3281–3287.

[17] L. Feuz, P. Jönsson, M.P. Jonsson, F. Höök. Improving the limit of detection of nanoscale sensors by directed binding to high-sensitivity areas. *ACS Nano*, **2010**, *4*, 2167–2177.

[18] D. Burdinski, M. Saalmink, J.P.W.G. van den Berg, C. van den Marel. Universal ink for microcontact printing. *Angew. Chem. Int. Ed.*, **2006**, *26*, 4355–4358.

[19] F. Palazon, D. Léonard, T.L. Mogne, F. Zuttion, C. Chevalier, M. Phaner-Goutorbe, É. Souteyrand, Y. Chevolot, J.P. Cloarec. Orthogonal chemical functionalization of patterned gold on silica surfaces. *Beilstein J Nanotechnol.*, **2015**, *6*, 2272–2277.

[20] M. Palma, J.J. Abramson, A.A. Gorodetsky, E. Penzo, R.L. Gonzalez, Jr., M.P. Sheetz, C. Nuckolls, J. Hone, S.J. Wind. Selective biomolecular nanoarrays for parallel single-molecule investigations. *J. Am. Chem. Soc.*, **2011**, *133*, 7656–7659.

[21] E. Briand, V. Humblot, J. Landoulsi, S. Petronis, C.M. Pradier, B. Kasemo, S. Svedhem. Chemical modifications of Au/SiO_2 template substrates for patterned biofunctional surfaces. *Langmuir*, **2011**, *27*, 678–685.

[22] H.G. Cai, S.J. Wind. Improved glass surface passivation for single-molecule nanoarrays. *Langmuir*, **2016**, *32*, 10034–10041.

[23] F. Battegay, M. Fourel. Barrier material selection for TSV last, flipchip & 3D-UBM & RDL integrations. *IEEE Electronic Components and Technology Conference* (*ECTC)*, **2015**, 1183–1192.

[24] C.K. Wang, S.J. Chang, Y.K. Su, C.S. Chang, Y.Z. Chiou, C.H. Kuo, T.K. Lin, T.K. Ko, J.J. Tang. GaN MSM photodetectors with TiW transparent electrodes. *Mater. Sci. Eng. B*, **2004**, *112*, 25–29.

[25] A. Roshanghias, G. Khatibi, R. Pelzer, J. Steinbrenner. On the effects of thickness on adhesion of TiW diffusion barrier coatings in silicon integrated circuits. *Surf. Coat. Technol.*, **2014**, *259*, 386–392.

[26] S.K. Bhagat, N.D. Theodore, T.L. Alford. Thermal stability of tungsten–titanium diffusion barriers for silver metallization. *Thin Solid Films*, **2008**, *516*, 7451–7457.

[27] S.Q. Wang, S. Suthar, C. Hoeflich, B. Burrow. Diffusion barrier properties of TiW between Si and Cu. *J. Appl. Phys.*, **1993**, *73*, 2301–2320.

[28] H.C. Chiua, C.H. Chen, C.W. Yang, H.L. Kao, F.H. Huang, S.W. Peng. Highly thermally stable in situ SiN_X passivation AlGaN/GaN enhancement-mode high electron mobility transistors using TiW refractory gate structure. *J. Vac. Sci. Technol. B*, **2013**, *31*, 051212 1–4.

[29] J.C. Chiou, K.C. Juang, M.C. Chen. TiW (N) as diffusion barriers between Cu and Si. *J. Electrochem. Soc.*, **1995**, *142*, 2326–2331.

[30] A. Maalaoui, M. Frenea-robin, J. Genest, S. Ecoffey, J. Beauvais, P. Charette, D. Drouin, J.P. Cloarec. *IEEE International Conference on Industrial Technology (ICIT)*, **2018**, 1350-1354.

[31] T.J. Daou, S. Begin-Colin, J.M. Greneche, F. Thomas, A. Derory, P. Bernhardt, P. Legare, G. Pourroy. Phosphate adsorption properties of magnetite-based nanoparticles. *Chem. Mater.*, **2007**, *19*, 4494–4505.

[32] D. Toulemon, B.P. Pichon, X. Cattoën, M.W.C. Man, S. Begin-Colin. 2D assembly of non-interacting magnetic iron oxide nanoparticlesvia “click” chemistry. *Chem. Commun.*, **2011**, *47*, 11954–11956.

[33] T. Patois, A.E. Taouil, F. Lallemand, L. Carpentier, X. Roizard, J.Y. Hihn, V. Bondeau-Patissier, Z. Mekhalif. Microtribological and corrosion behaviors of 1H,1H,2H,2H-perfluorodecanethiol self-assembled films on copper surfaces. *Surf. Coat. Technol.*, **2010**, *205*, 2511–2517.

[34] F. Laffineur, D. Auguste, F. Plumier, C. Pirlot, L. Hevesi, J. Delhalle, Z. Mekhalif. Comparison between $CH_3(CH_2)_{15}SH$ and $CF_3(CF_2)_3(CH_2)_{11}SH$ monolayers on electrodeposited silver. *Langmuir*, **2004**, *20*, 3240–3245.

[35] F. Brétagnol, L. Ceriotti, A. Valsesia, T. Sasaki, G. Ceccone, D. Gilliland, P. Colpo, F. Rossi. Fabrication of functional nano-patterned surfaces by a combination of plasma processes and electron-beam lithography. *Nanotechnology*, **2007**, *18*, 135303.

[36] A.V. Ievlev, M. Chyasnavichyus, D.N. Leonard, J.C. Agar, G.A. Velarde, L.W. Martin, S.V. Kalinin, P. Maksymovych, O.S. Ovchinnikova. Subtractive fabrication of ferroelectric thin films with precisely controlled thickness. *Nanotechnology*, **2018**, *29*, 155302.

[37] B.R. Chakraborty, D. Haranath, H. Chander, S. Hellweg, S. Dambach, H.F. Arlinghaus. TOF-SIMS and laser-SNMS investigations of dopant distribution in nanophosphors. *Nanotechnology*, **2005**, *16*, 1006.

[38] E.E. Bedford, S. Boujday, V. Humblot, F.X. Gu, C.M. Pradier. Effect of SAM chain length and binding functions on protein adsorption: β-Lactoglobulin and apo-transferrin on gold. *Colloids Surf. B Biointerfaces*, **2014**, *116*, 489–496.

[39] C.D. Bain, E.B. Troughton, Y.T. Tao, J. Evall, G.M. Whitesides, R.G. Nuzzo. Formation of monolayer films by the spontaneous assembly of organic thiols from solution onto gold. *J. Am. Chem. Soc.*, **1989**, *111*, 321–335.

[40] R.G. Nuzzo, B.R. Zegarski, L.H. Dubois. Fundamental studies of the chemisorption of organosulfur compounds on gold (111). Implications for molecular self-assembly on gold surfaces. *J. Am. Chem. Soc.*, **1987**, *109*, 733–740.

[41] Z.G. Yang, Y. Chevolot, T. Géhin, V. Dugas, N. Xanthopoulos, V. Laporte, T. Delair, Y. Ataman-Önal, G. Choquet-Kastylevsky, É. Souteyrand, E. Laurencea. Characterization of three amino-functionalized surfaces and evaluation of antibody immobilization for the multiplex detection of tumor markers involved in colorectal cancer. *Langmuir*, **2013**, *29*, 1498–1509.